NANO LETTERS

pubs.acs.org/NanoLett

Letter

On-Chip Topological Photonic Crystal Nanobeam Filters

Mo-Dian Liu,[▽] Hou-Hong Chen,[▽] Ziyu Wang,* Yong Zhang, Xin Zhou, Guo-Jing Tang, Fei Ma, Xin-Tao He, Xiao-Dong Chen,* and Jian-Wen Dong*

Cite This: *Nano Lett.* 2024, 24, 1635−1641

Read Online

ACCESS | Metrics & More | Article Recommendations | Supporting Information

ABSTRACT: We present an on-chip filter with a broad tailorable working wavelength and a single-mode operation. This is realized through the application of topological photonic crystal nanobeam filters employing synthesis parameter dimensions. By introducing the translation of air holes as a new synthetic parameter dimension, we obtained nanobeams with tunable Zak phases. Leveraging the bulk-edge correspondence, we identify the existence of topological cavity modes and establish a correlation between the cavity's interface morphology and working wavelength. Through experiments, we demonstrate filters with adjustable filtering wavelengths ranging from 1301 to 1570 nm. Our work illustrates the use of the synthetic translation dimension in the design of on-chip filters, and it holds potential for applications in other devices such as microcavities.

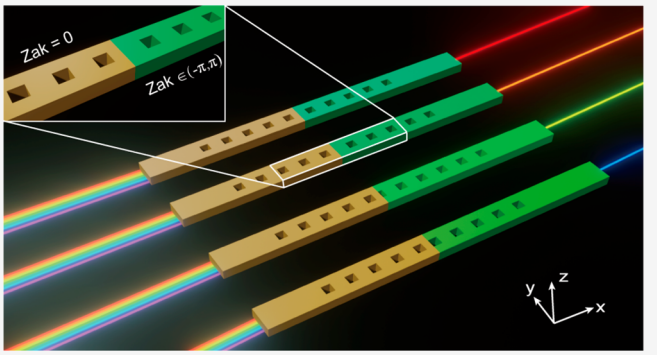

KEYWORDS: *topological photonics, synthetic parameter dimensions, photonic crystal nanobeam, on-chip filter*

On-chip filters are integrated components in various nanophotonics devices, including wavelength division multiplexers and spectrometers. Their integration into these devices facilitates the precise control of light within specific wavelength ranges.[1−11] Photonic crystals (PCs) have emerged as a prominent platform for designing on-chip filters. PCs are artificial optical materials with periodic structures that exhibit a band gap in which the propagation of light is forbidden.[12,13] Via the introduction of defects into the bulk PCs, photonic cavities can be formed, enabling the selective transmission or blocking of certain wavelengths.[14−21] PC-based filters offer the advantage of miniaturization and precise control over the transmission spectrum by adjusting the structural parameters of the introduced defects. This tailorable spectral response enables customized filtering characteristics. However, it is important to note that the tailorable spectral response of PC-based filters is constrained by the available parameters, which may limit the range of achievable filtering capabilities.

In the past few years, topological photonic crystals (TPCs) have attracted a great deal of attention with exciting prospects for controlling light in novel ways.[22−27] For example, unidirectional backscattering-immune propagation of light and topological midgap defect modes have been demonstrated.[28−32] High-performance nanophotonic on-chip devices, such as robust waveguides and topological cavities,[33−38] have also been proposed and realized. However, the realization of topological nanophotonic crystal devices remains challenging, primarily due to material constraints and the complexity of their design. Recent advancements in the field have introduced the concept of synthetic dimensions, which allows for the exploration of topological physics in higher-dimensional spaces beyond the traditional geometrical dimensionality of the structures.[39−48] This innovative approach simplifies the design of on-chip TPC devices by eliminating the reliance on specific symmetry protection or stringent material requirements.[49−51] By incorporating synthetic dimensions, researchers have opened up new possibilities for realizing practical topological nanophotonic crystal devices.

In this work, we realize on-chip TPC nanobeam filters based on the synthetic parameter dimension. Our design approach involves the utilization of Zak phases to engineer the topological properties of the PC nanobeams. The Zak phase quantifies how the wave function changes as the momentum varies across the Brillouin zone and helps to determine whether a PC nanobeam is topological (see eq 1 for details). Additionally, we consider the translation of the air holes as an additional degree of freedom, enabling the realization of PC nanobeams with different Zak phases. Leveraging the bulk-edge correspondence principle, we identify the presence of topological cavity modes and establish a relationship between

Received: November 12, 2023
Revised: January 23, 2024
Accepted: January 23, 2024
Published: January 26, 2024

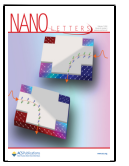

https://doi.org/10.1021/acs.nanolett.3c04363
Nano Lett. 2024, 24, 1635−1641

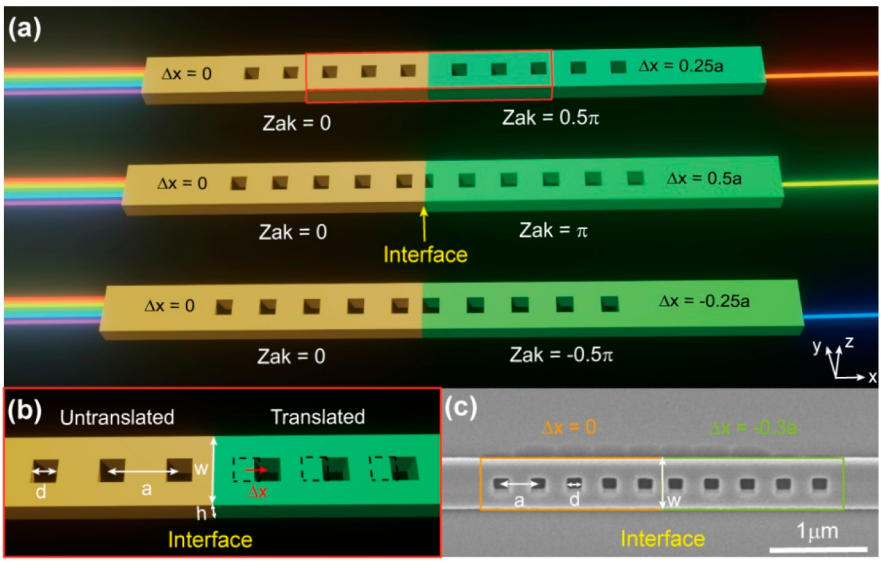

Figure 1. Schematic of topological photonic crystal (TPC) nanobeam filters. (a) Schematic of three different TPC nanobeam filters. The air holes in the left part of the nanobeam (highlighted in yellow) are untranslated, leading to a trivial PC nanobeam with a Zak phase of zero. On the contrary, the air holes in the right part (highlighted in green) are translated by Δx, creating a PC nanobeam characterized with a non-zero Zak phase. From top to bottom, the translation of air holes (i.e., Δx) at the right part is $0.25a$, $0.5a$, and $-0.25a$, respectively. (b) Schematic of the topological cavity that is composed of two PC nanobeams with different translations. Structural parameters: lattice constant a = 380 nm, width w = 500 nm, height h = 220 nm, and side length of square air hole d = 170 nm. (c) Top view of the scanning electron microscope image of a fabricated topological cavity with $\Delta x = 0$ and $\Delta x = -0.3a$.

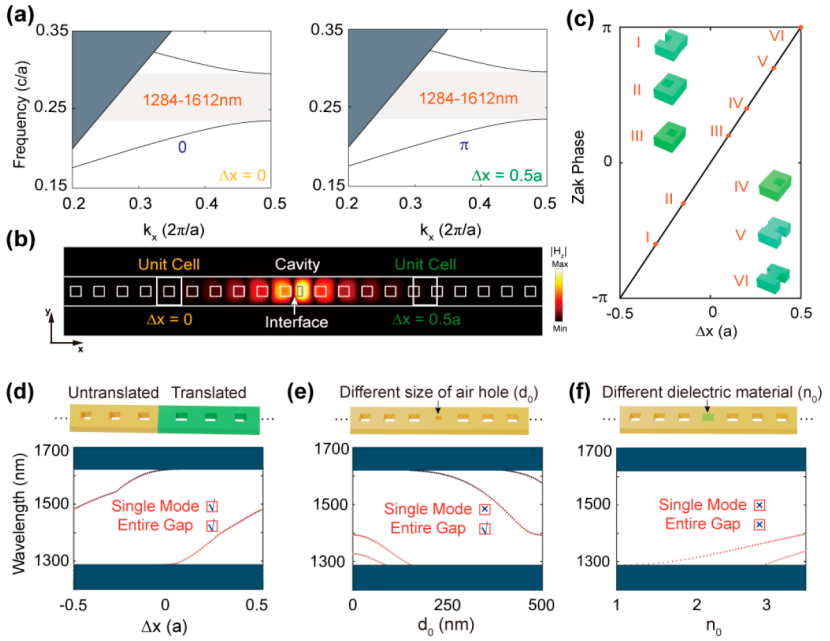

Figure 2. Design scheme of the topological PC nanobeam cavity. (a) Bulk bands of the TE-like mode of the PC nanobeam. A band gap is highlighted in gray. The Zak phase of first band is marked with blue letters. (b) $|H_z|$ field of the topological cavity mode of a representative interface between the PC nanobeam with $\Delta x = 0$ and the PC nanobeam with $\Delta x = 0.5a$. (c) Zak phase as a function of translation (Δx). The inset shows unit cells of PC nanobeams with different translations, i.e., (I) $\Delta x = -0.3a$, (II) $\Delta x = -0.15a$, (III) $\Delta x = -0.1a$, (IV) $\Delta x = 0.2a$, (V) $\Delta x = 0.35a$, (VI) $\Delta x = 0.5a$, and (VII) $\Delta x = 0.5a$. (d) Band dispersion of topological cavity modes as a function of the translation of the air hole (i.e., Δx). (e and f) Band dispersions of cavity modes as a function of size length d_0 and refractive index n_0 of the center air hole, respectively.

the wavelength of topological cavity modes and the translation of the PC nanobeam's air holes. To validate our findings, we fabricate nanophotonic samples and record transmission spectra. By checking PC nanobeams with varying translations, we observe distinct filtering wavelengths in the spectra, showcasing the broad tailorable working wavelength spanning the entire band gap and the achievement of single-mode operation. Our work demonstrates the implementation of on-chip TPC nanobeam filters by leveraging the concept of synthetic parameter dimension and opens up new possibilities for the development of advanced nanophotonic devices with tailored spectral responses.

To illustrate our concept, we present a schematic of the designed TPC nanobeam filters under translational deforma-

https://doi.org/10.1021/acs.nanolett.3c04363
Nano Lett. 2024, 24, 1635−1641

tions (Figure 1a). The considered PC nanobeam has periodic air holes along the propagation direction of light (x), but it has finite sizes along other directions (y and z). The structural parameters, namely, a, w, h, and d, correspond to the lattice constant, the width of the nanobeam, the thickness of the nanobeam, and the size length of air holes, respectively. To create a cavity, we introduce a translation (Δx) to the air holes within the right PC nanobeam (highlighted in green) and subsequently connect the untranslated and translated PC nanobeams (Figure 1b). Because these two PC nanobeams are characterized by different Zak phases (see more details in section 1 of the Supporting Information), the interface between them will support a localized topological cavity mode due to the bulk-edge correspondence. By considering interfaces with different translations, we can realize TPC nanobeam filters that filter out specific wavelengths. In contrast to conventional nanobeam filters, the designed TPC nanobeam filters exhibit several advantages. One key advantage is their tunability of the working wavelength, crossing the entire band gap, allowing for flexibility in choosing the desired operating wavelength. Additionally, TPC nanobeam filters operate in a single-mode regime, ensuring a clean and well-defined output signal. The following paragraphs provide further demonstrations and evidence of these advantages.

For the sake of concreteness, we consider a PC nanobeam with a = 380 nm, w = 500 nm, h = 220 nm, and d = 170 nm. The unit cells of two representative structures, namely, nanobeams with $\Delta x = 0$ and $\Delta x = 0.5a$, are shown in the insets of Figure 2a. They have identical bulk bands, featuring a band gap spanning from 1284 to 1612 nm (i.e., a very large bandwidth of 328 nm, covering a majority of the O band, the entire E band, the entire S band, the entire C band, and a majority of the L band of optical communication). However, these two bulk bands have different topological properties that are characterized by the Zak phases:[52,53]

$$\theta^{\mathrm{Zak}} = \int_{-\pi/a}^{\pi/a} \left[i \int_{-a/2}^{a/2} u_{k_x}^{*}(x)\varepsilon(x)\partial_{k_x} u_{k_x}(x)\, \mathrm{d}x \right] \mathrm{d}k_x \tag{1}$$

where $\varepsilon(x)$ is the relative permittivity and $u_{k_x}(x)$ is the normalized periodic part of the electric field of Bloch wave function with wave vector k_x. On the basis of eq 1, we determine that the Zak phase of the first band for PC nanobeam with $\Delta x = 0$ ($\Delta x = 0.5a$) is 0 (π). Due to the topological difference between these two PC nanobeams, the existence of a cavity mode located at the center of bulk band gap is guaranteed by topology. To verify this, we construct an interface by placing the nanobeam with $\Delta x = 0$ at the left and the nanobeam with $\Delta x = 0.5a$ at the right. Numerical results show that there is a cavity mode with its wavelength (1483 nm) located within the bulk band gap and its $|H_z|$ field localizing at the interface (Figure 2b).

To present the tunability of the wavelength of the topological cavity mode, we introduce translational deformation to the PC nanobeam at the right of the interface. Here, we consider six unit cells with different translations (insets of Figure 2c), and these unit cells correspond to the experimental samples, which will be discussed in Figure 3d. For each PC nanobeam with a different Δx, the Zak phase of the first bulk band is defined as

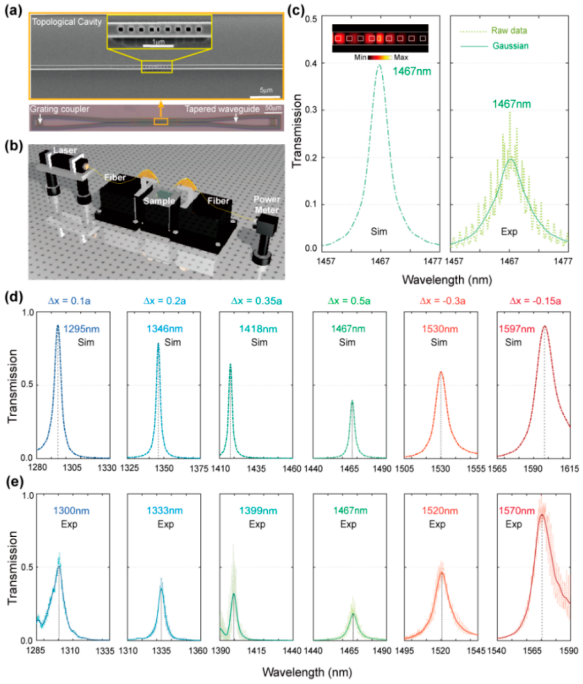

Figure 3. Observation of the cavity mode of TPC nanobeam filters. (a) Optical micrograph of the fabricated TPC nanobeam filter between PC nanobeams with $\Delta x = 0$ and $\Delta x = 0.5a$. The inset shows a close-up SEM image of the suspended topological cavity with a period N of 8. (b) Schematic diagram of the experimental setup. (c) Transmission spectrum of the TPC nanobeam filter in panel b. The green dashed line represents the simulation result, with the inset displaying the calculated $|H_z|$ field of the topological cavity mode. The green dashed line corresponds to the measured transmission spectrum, while the green solid line represents the transmission spectrum obtained by fitting the raw data with a Gaussian filter. (d) Simulation transmission spectra of the TPC nanobeam filter with different translations. (e) Measured transmission spectra of the TPC nanobeam filter with different translations. The dashed line represents the raw data, while the solid line corresponds to the data after the Gaussian filter. The transmission spectrum for the TPC nanobeam filter with $\Delta x = 0.5a$ is shown as an example in panel c.

$$\theta^{\mathrm{Zak}}(\Delta x) = \int_{-\pi/a}^{\pi/a} \left[i \int_{-a/2}^{a/2} u_{k_x}^{*}(x, \Delta x)\varepsilon(x, \Delta x) \times \partial_{k_x} u_{k_x}(x, \Delta x)\, \mathrm{d}x \right] \mathrm{d}k_x \tag{2}$$

where the translated $\varepsilon(x, \Delta x) = \varepsilon(x - \Delta x)$, and $u_{k_x}(x, \Delta x) = u_{k_x}(x - \Delta x)\mathrm{e}^{-ik_x\Delta x}$. The calculated results show that each nanobeam is characterized by a non-zero Zak phase, which is linearly proportional to Δx. As Δx changes by one lattice constant, the PC nanobeam goes back to itself and the Zak phase evolves 2π (Figure 2c):

$$\theta^{\mathrm{Zak}}(\Delta x) = \theta^{\mathrm{Zak}}(0) + 2\pi/a \tag{3}$$

As translation Δx varies from $-a/2$ to $a/2$ and is independent of other variables, it can be treated as a synthetic parameter and understood as a pseudomomentum.[49,54,55] Therefore, we can define a two-dimensional (2D) parameter space spanned by one Bloch momentum (k_x) and one pseudomomentum (Δx). In this closed 2D parameter space (k_x, Δx), the topological invariant, i.e., Chern number, is related to the evolution of the Zak phase when Δx changes by a period, as

https://doi.org/10.1021/acs.nanolett.3c04363
Nano Lett. 2024, 24, 1635−1641

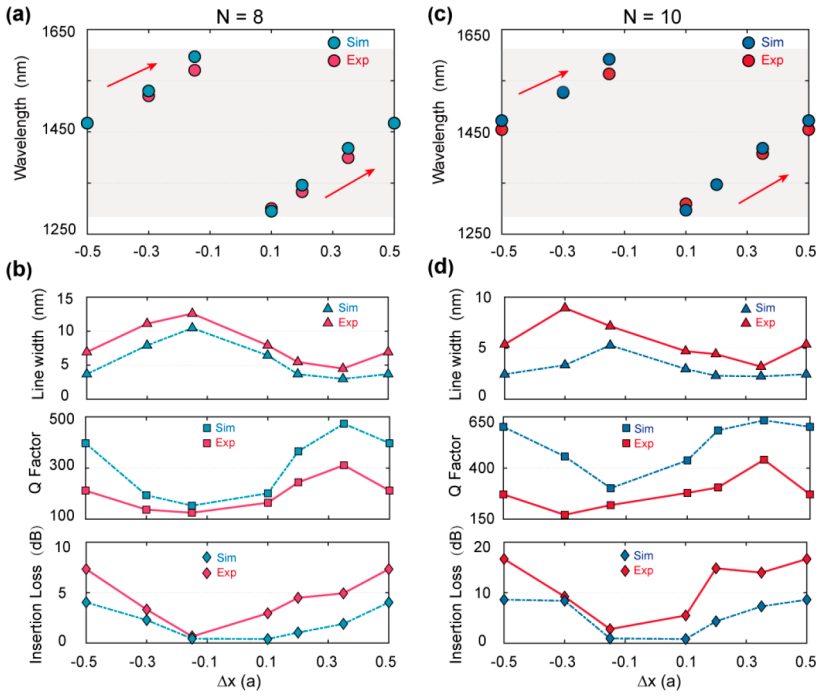

Figure 4. Optical characterization of TPC nanobeam filters. Filtering wavelengths of TPC nanobeam filters with periods of (a) 8 and (c) 10. Blue circles represent simulation results of TPC nanobeam filters, and red circles represent measured results. The red arrows indicate the trend of the wavelength variation. Line widths, quality factors, and insertion losses of the TPC nanobeam filters with periods of (b) 8 and (d) 10. Blue dashed lines represent simulation results, while red solid lines represent measured results.

shown by $C = -\frac{1}{2\pi}\int \partial_{\Delta x}\theta^{\mathrm{Zak}}(\Delta x)\,\mathrm{d}\Delta x = -1$. In this context, the translated and untranslated PC nanobeams manifest topological and trivial structures, respectively. Due to the principle of bulk-edge correspondence, gapless cavity modes traverse the bulk band gap when Δx completes a period. This intriguing phenomenon enables the emergence of a tunable topological cavity mode when two PC nanobeams with differing Zak phases are combined.

The proposed topological cavity offers several advantages over traditional PC nanobeam cavities designed by other alternative methods. Specifically, it enables a broader tunable working wavelength range and single-mode operation. To clearly demonstrate these advantages, we compare the wavelength dispersions of cavity modes designed by using three different methods. First, we consider the interface between two PC nanobeams with different Zak phases (Figure 2d). When translation Δx varies from $-a/2$ to $a/2$ (i.e., −190 to 190 nm), the topological cavity mode gradually traverses the entire gap, akin to conventional topological pumping.[49] Moreover, at each specific translation, the topological cavity exclusively supports a single mode, ensuring a clean and well-defined output signal. As a comparison, we also investigate two alternative cavity design methods. To be fair, we consider the PC nanobeam with identical structural parameters (lattice constant, width, thickness, and air hole size) and introduce the defect by disturbing the center air hole in the middle of nanobeam (top panel of panels e and f of Figure 2). In Figure 2e, we create a cavity by modifying the size (d_0) of the center air hole in the PC nanobeam. By considering d_0 from 0 to 500 nm, we analyze all possible defect cases and observe that the cavity modes cover the entire band gap. Once d_0 gradually increases, the cavity modes become insufficiently localized. Consequently, energy within the cavity will leak from the sidewall into the surrounding air (more details in section 2 of the Supporting Information). In Figure 2f, the other kind of cavity is created by filling the center air hole of the PC nanobeam with a dielectric material with refractive index n_0. By varying n_0 from 1 to 3.5 (corresponding to the refractive index range of the standard on-chip materials), we find that the wavelengths of the cavity mode cover only 33% of the band gap. Additionally, these two design methods cannot ensure single-mode operation, while our topological cavity can. Note that one-dimensional arrays with two quantized Zak phases (i.e., 0 or π) and their associated topological interface mode have been reported,[52,53] but our work introduces a unit cell that breaks the mirror symmetry, resulting in Zak phases spanning any real number within the range of $[-\pi, \pi]$. The topological cavities constructed through the translation method support cavity modes spanning the entire band gap and enable single-mode operation. This is topologically protected, because the Chern number within the 2D synthetic space is inherently non-zero. It cannot be achieved in other cavities constructed through the hole or dielectric defection insertion methods (another example in section 3 of the Supporting Information). Therefore, in the following experiment, we focus on the topological cavity under translation deformation.

To confirm the theoretical findings, we conducted experimental demonstrations in the optical wavelength range based on the silicon-based nanophotonic structure. The fabricated PC nanobeam has a number of periods (N) of 8, and the top panel of Figure 3a shows the SEM image of one sample. To ensure efficient coupling between modes in the optical fiber and waveguide, we integrate two grating couplers at both the input and output ends of the PC nanobeam filter (bottom panel of Figure 3a). Between the grating coupler and the topological cavity, a tapered waveguide is designed to

https://doi.org/10.1021/acs.nanolett.3c04363
Nano Lett. 2024, 24, 1635−1641

improve the coupling efficiency and reduce reflection losses. The experimental setup is depicted in Figure 3b. As an example, we consider the sample between PC nanobeams with $\Delta x = 0$ and $\Delta x = 0.5a$ (i.e., the structure depicted in Figure 3a). Figure 3c illustrates the simulated and experimental transmission spectra. In the simulated spectrum, a transmission peak is observed at 1467 nm. We also analyzed the excitation field at this wavelength, as shown in the inset of Figure 3c. The analysis reveals that the energy is primarily concentrated near the interface, which aligns well with our theoretical prediction in Figure 2f. Notably, the leftmost energy localization within the PC nanobeam corresponds to the entrance of the incident light. Considering the experimental results, we apply a Gaussian filter (more details in section 4 of the Supporting Information) to the raw spectrum (the green dotted line) to remove the Fabry−Pérot fringes resulting from the reflections at the grating couplers. Note that in the experiment one method for reducing the fringes of the measured transmission spectra is to improve the coupling efficiency between the incident fiber and the grating coupler. This can be done by modifying the coupling angle between the fiber and the on-chip grating coupler. The resultant transmission spectrum is represented by the green solid line, and it shows one transmission peak at 1467 nm, which coincides with the simulated one.

To extend the wavelength coverage within the band gap, we fabricated TPC nanobeam filters with different translations. Simultaneously, we conducted simulations for the transmission spectrum of TPC nanobeam filters under various translations (Figure 3d). Note that as the working bandwidth of the input and output grating couplers is ∼100 nm and the bandwidth of the band gap is 328 nm, we design three grating couplers with different center working wavelengths for TPC nanobeam filters with different working wavelengths (more details in section 5 of the Supporting Information). The transmission spectra of TPC nanobeam filters with varying Δx values are presented in panels d and e of Figure 3. Upon comparing the simulation and measured results, we observed a wavelength shift, which could be attributed to variations in the size of the air holes in the samples during fabrication, differing from the intended design. As Δx varies, we observe a corresponding shift in the measured wavelength of the transmission peak, from 1300 to 1570 nm.

Moreover, we conducted a comparison with the TPC nanobeam filter with an N of 10 (see Figure S4). For the sake of clarity, we summarize the relation between the translation of air holes and the corresponding transmission peak at different periods (Figure 4a,c). As Δx increases from $-0.5a$ to 0 (or from 0 to $0.5a$), the transmission peak experiences a red-shift, irrespective of whether the periodicity is 8 or 10. This behavior is consistent in both the simulation and experimental results. Additionally, we evaluate the performance of the TPC nanobeam filters by analyzing the line width, quality factor (Q), and insertion loss (Figure 4b,d). With an increase in the number of periods, we observe a reduction in the line width of the TPC nanobeam filter, while Q tends to increase for periodicities of both 8 and 10. The line width/Q competes with insertion loss, and this trend is also observed in both simulation and experimental results. The minimum insertion loss of our designed TPC nanobeam filter reaches 0.65 dB for $\Delta x = -0.15a$, and the minimum filtering line width is 3.2 nm for $\Delta x = 0.35a$. In our work, the quality factor of the transmission peak is not large (∼300), the bandwidth is not narrow (∼3 nm), and the insertion loss is large. This is because the band gap discussed in our work is extremely wide. If the band gap is reduced, the performance of the filter will be improved (more details in section 6 of the Supporting Information). To expand the functionality of our TPC nanobeam filters and cater to scenarios where filtering information at multiple wavelengths is required, we explore the possibility of cascading two PC nanobeam cavities (more details in section 7 of the Supporting Information).

In summary, we have realized TPC nanobeam filters under translational deformations. The introduction of translation, serving as a synthetic parameter dimension, allows us to establish a clear correlation between the topological cavity morphology and the corresponding wavelength. Extensive theoretical analysis and experimental investigations have demonstrated the ability to tune the filtering wavelength across the entire band gap by adjusting the positions of the air holes within one period. We achieve a minimal insertion loss of <1 dB and a minimum line width of 3.2 nm. These significant achievements highlight the potential application of topological physics in integrated nanophotonics. The topological method based on synthetic dimensions imposes no restrictions on lattice types, symmetries, or materials, making it adaptable for on-chip device design. This work serves as an illustration of incorporating synthetic translation dimensions in the creation of on-chip filters, with potential applications extending to other devices like microcavities.

METHODS

Numerical Simulation. The finite-element method solver COMSOL Multiphysics is employed for the numerical modeling of the PC nanobeam. The relative permittivity of silicon is assumed to be constant at 12 across the entire spectral range of interest. To calculate the band structures (Figure 2a), eigenfrequency analyses are conducted in a three-dimensional (3D) configuration. The 3D eigenmode solver is utilized to numerically simulate the cavity mode of the PC nanobeam cavity (Figure 2b). Furthermore, to validate the transmittance spectra of PC nanobeams under different translation and the excited cavity mode of the PC nanobeam filter, finite-difference time-domain calculations are performed by using Lumerical FDTD Solutions. We utilized FDTD to acquire the transmission spectrum of the TPC nanobeam filter. We put the incidence of the TE mode placed right before the first air hole, and the monitor is placed right after the last air hole (Figure 3d). Our calculation method for Q and insertion loss (IL) follows a common approach. Q is calculated as the resonant wavelength divided by the full width at half-maximum, and IL is determined using the formula IL (decibels) = $-10 \times \log_{10}$(transmittance) (Figure 4b,d).

Sample Fabrication. The devices were fabricated on a commercially available silicon-on-insulator (SOI) wafer. The silicon layer had a thickness of 220 nm, while the buried silica layer had a thickness of 2 μm. Initially, electron-beam lithography (EBL) was employed to define the waveguides and air holes on an electron-beam resist, called AR-P 6200. Subsequently, these patterns were transferred to the silicon layer through an inductively coupled plasma (ICP) etching process, resulting in an etching depth of 220 nm. Next, grating couplers were defined on the silicon layer by using the aligned EBL and an ICP etching process, resulting in an etching depth of 70 nm. Following this, the aligned EBL was used again to define the region for wet etching on the electron-beam resist [poly(methyl methacrylate) (PMMA)]. The resist was then

https://doi.org/10.1021/acs.nanolett.3c04363
Nano Lett. 2024, 24, 1635−1641

subjected to development and hard-bake processes. Wet etching with hydrofluoric acid was carried out in this defined region to create the suspended structures. Finally, the resist was removed entirely to conclude the fabrication process.

Optical Measurements. The optical sources used in the experiment consisted of three tunable continuous wave (CW) lasers (Santec TSL-550/710) operating in the telecom wavelength range of 1260−1640 nm. To initiate the measurements, the incident light was launched into the input fiber and subsequently coupled to the waveguide by using the input grating coupler. The light then traversed through the PC nanobeam filter before exiting into the output fiber via the output grating coupler. To capture the transmission spectra, the wavelength of the CW laser was automatically tuned in increments of 10 pm. The detection of these spectra was achieved by using an optical power meter (MPM-210). During the experimental measurements, reference samples were prepared. In our measurements, we acquired transmission spectra for both the reference sample and the TPC nanobeam filter sample. Subsequently, the transmission spectrum of the reference sample was normalized to derive the final transmission spectrum for the TPC nanobeam filter (Figure 3e).

■ ASSOCIATED CONTENT

Supporting Information

The Supporting Information is available free of charge at https://pubs.acs.org/doi/10.1021/acs.nanolett.3c04363.

> Additional information about the Zak phase of nanobeams with different translations, eigen field of cavity modes of the PC nanobeam cavity with a large d_0, single-mode-ness and wide control of the topological cavity mode, method of the Gaussian filter, design of the grating coupler, route for improving Q and reducing the filter line width and insertion loss of the filter, and cascaded TPC nanobeam filters (PDF)

■ AUTHOR INFORMATION

Corresponding Authors

Ziyu Wang − *The Institute of Technological Sciences, Wuhan University, Wuhan 430072, China;* orcid.org/0000-0001-9718-1263; Email: zywang@whu.edu.cn

Xiao-Dong Chen − *School of Physics & State Key Laboratory of Optoelectronic Materials and Technologies, Sun Yat-sen University, Guangzhou 510275, China;* orcid.org/0000-0001-8698-0609; Email: chenxd67@mail.sysu.edu.cn

Jian-Wen Dong − *School of Physics & State Key Laboratory of Optoelectronic Materials and Technologies, Sun Yat-sen University, Guangzhou 510275, China;* orcid.org/0000-0003-2379-554X; Email: dongjwen@mail.sysu.edu.cn

Authors

Mo-Dian Liu − *School of Physics & State Key Laboratory of Optoelectronic Materials and Technologies, Sun Yat-sen University, Guangzhou 510275, China*

Hou-Hong Chen − *School of Physics & State Key Laboratory of Optoelectronic Materials and Technologies, Sun Yat-sen University, Guangzhou 510275, China*

Yong Zhang − *State Key Laboratory of Advanced Optical Communication Systems and Networks, Department of Electronic Engineering, Shanghai Jiao Tong University, Shanghai 200240, China*

Xin Zhou − *School of Physics & State Key Laboratory of Optoelectronic Materials and Technologies, Sun Yat-sen University, Guangzhou 510275, China*

Guo-Jing Tang − *School of Physics & State Key Laboratory of Optoelectronic Materials and Technologies, Sun Yat-sen University, Guangzhou 510275, China*

Fei Ma − *School of Physics & State Key Laboratory of Optoelectronic Materials and Technologies, Sun Yat-sen University, Guangzhou 510275, China*

Xin-Tao He − *School of Physics & State Key Laboratory of Optoelectronic Materials and Technologies, Sun Yat-sen University, Guangzhou 510275, China*

Complete contact information is available at: https://pubs.acs.org/10.1021/acs.nanolett.3c04363

Author Contributions

▽M.-D.L. and H.-H.C. contributed equally to this work.

Notes

The authors declare no competing financial interest.

■ ACKNOWLEDGMENTS

This work was supported by the National Key Research & Development Program of China (2022YFA1404304), the National Natural Science Foundation of China (12074443, 12374364, 62035016, 62105374, and 12274475), the Guangdong Basic and Applied Basic Research Foundation (2023B1515040023, 2023A1515012723, and 2023B1515020072), the Fundamental Research Funds for the Central Universities, and Sun Yat-sen University (23lgbj021).

■ REFERENCES

(1) Elshaari, A. W.; Zadeh, I. E.; Fognini, A.; Reimer, M. E.; Dalacu, D.; Poole, P. J.; Zwiller, V.; Jons, K. D. On-chip single photon filtering and multiplexing in hybrid quantum photonic circuits. *Nat. Commun.* **2017**, *8*, 379.

(2) Zhang, W.; Yao, J. On-chip silicon photonic integrated frequency-tunable bandpass microwave photonic filter. *Opt. Lett.* **2018**, *43*, 3622−3625.

(3) Jia, H.; Yang, S.; Zhou, T.; Shao, S.; Fu, X.; Zhang, L.; Yang, L. WDM-compatible multimode optical switching system-on-chip. *Nanophotonics* **2019**, *8*, 889−898.

(4) Oser, D.; Mazeas, F.; Le Roux, X.; Pérez-Galacho, D.; Alibart, O.; Tanzilli, S.; Labonté, L.; Marris-Morini, D.; Vivien, L.; Cassan, É.; Alonso-Ramos, C. Coherency-Broken Bragg Filters: Overcoming On-Chip Rejection Limitations. *Laser Photonics Rev.* **2019**, *13*, No. 1800226.

(5) Harvey-Collard, P.; Zheng, G.; Dijkema, J.; Samkharadze, N.; Sammak, A.; Scappucci, G.; Vandersypen, L. M. K. On-Chip Microwave Filters for High-Impedance Resonators with Gate-Defined Quantum Dots. *Physical Review Applied* **2020**, *14*, No. 034025.

(6) Li, A.; Fainman, Y. On-chip spectrometers using stratified waveguide filters. *Nat. Commun.* **2021**, *12*, 2704.

(7) Cheng, Z.; Zhao, Y.; Zhang, J.; Zhou, H.; Gao, D.; Dong, J.; Zhang, X. Generalized Modular Spectrometers Combining a Compact Nanobeam Microcavity and Computational Reconstruction. *ACS Photonics* **2022**, *9*, 74−81.

(8) Zhang, Z.; Liu, Y.; Wang, Z.; Zhang, Y.; Guo, X.; Xiao, S.; Xu, K.; Song, Q. Folded Digital Meta-Lenses for on-Chip Spectrometer. *Nano Lett.* **2023**, *23*, 3459−3466.

(9) Kong, L.; Zhao, Q.; Wang, H.; Guo, J.; Lu, H.; Hao, H.; Guo, S.; Tu, X.; Zhang, L.; Jia, X.; Kang, L.; Wu, X.; Chen, J.; Wu, P. Single-Detector Spectrometer Using a Superconducting Nanowire. *Nano Lett.* **2021**, *21*, 9625−9632.

(10) Jung, Y.; Jung, H.; Choi, H.; Lee, H. Polarization Selective Color Filter Based on Plasmonic Nanograting Embedded Etalon Structures. *Nano Lett.* **2020**, *20*, 6344−6350.
(11) Hyun, J. K.; Kang, T.; Baek, H.; Kim, D.-s.; Yi, G.-c. Nanoscale Single-Element Color Filters. *Nano Lett.* **2015**, *15*, 5938−5943.
(12) John, S. Strong localization of photons in certain disordered dielectric superlattices. *Phys. Rev. Lett.* **1987**, *58*, 2486.
(13) Yablonovitch, E. Inhibited spontaneous emission in solid-state physics and electronics. *Phys. Rev. Lett.* **1987**, *58*, 2059.
(14) Sepahvandi, V.; Rezaei, B.; Aly, A. H. Tunable multichannel Fibonacci one-dimensional terahertz photonic crystal filter. *Sci. Rep.* **2023**, *13*, 5631.
(15) Jalali Mehrabad, M.; Foster, A. P.; Martin, N. J.; Dost, R.; Clarke, E.; Patil, P. K.; Skolnick, M. S.; Wilson, L. R. Chiral topological add−drop filter for integrated quantum photonic circuits. *Optica* **2023**, *10*, 415−421.
(16) Dong, P.; Liu, C.; Zhang, L.; Dai, D.; Shi, Y. Reconfigurable add-drop filter based on an antisymmetric multimode photonic crystal nanobeam cavity in a silicon waveguide. *Opt. Express* **2022**, *30*, 17332−17339.
(17) Vasco, J. P.; Gerace, D.; Seibold, K.; Savona, V. Monolithic Silicon-Based Nanobeam Cavities for Integrated Nonlinear and Quantum Photonics. *Physical Review Applied* **2020**, *13*, No. 034070.
(18) Wang, Z.; Yi, S.; Chen, A.; Zhou, M.; Luk, T. S.; James, A.; Nogan, J.; Ross, W.; Joe, G.; Shahsafi, A.; Wang, K. X.; Kats, M. A.; Yu, Z. Single-shot on-chip spectral sensors based on photonic crystal slabs. *Nat. Commun.* **2019**, *10*, 1020.
(19) Dong, X.; Chi, J.; Zheng, L.; Ma, B.; Li, Z.; Wang, S.; Zhao, C.; Liu, H. Efficient isolation and sensitive quantification of extracellular vesicles based on an integrated ExoID-Chip using photonic crystals. *Lab Chip* **2019**, *19*, 2897−2904.
(20) Yang, Y.; Jiang, H.; Hang, Z. H. Topological Valley Transport in Two-dimensional Honeycomb Photonic Crystals. *Sci. Rep.* **2018**, *8*, 1588.
(21) Halimi, S. I.; Hu, S.; Afzal, F. O.; Weiss, S. M. Realizing high transmission intensity in photonic crystal nanobeams using a side-coupling waveguide. *Opt. Lett.* **2018**, *43*, 4260−4263.
(22) Ozawa, T.; Price, H. M.; Amo, A.; Goldman, N.; Hafezi, M.; Lu, L.; Rechtsman, M. C.; Schuster, D.; Simon, J.; Zilberberg, O.; Carusotto, I. Topological photonics. *Rev. Mod. Phys.* **2019**, *91*, No. 0156006.
(23) Kim, M.; Jacob, Z.; Rho, J. Recent advances in 2D, 3D and higher-order topological photonics. *Light: Sci. Appl.* **2020**, *9*, 130.
(24) Wang, H.; Gupta, S. K.; Xie, B.; Lu, M. Topological photonic crystals: a review. *Frontiers of Optoelectronics* **2020**, *13*, 50−72.
(25) Ma, S.; Yang, B.; Zhang, S. Topological photonics in metamaterials. *Photonics Insights* **2022**, *1*, R02.
(26) Tang, G. J.; He, X. T.; Shi, F. L.; Liu, J. W.; Chen, X. D.; Dong, J. W. Topological Photonic Crystals: Physics, Designs, and Applications. *Laser Photonics Rev.* **2022**, *16*, No. 2100300.
(27) You, J. W.; Lan, Z.; Ma, Q.; Gao, Z.; Yang, Y.; Gao, F.; Xiao, M.; Cui, T. J. Topological metasurface: from passive toward active and beyond. *Photonics Research* **2023**, *11*, B65.
(28) Wang, Z.; Chong, Y.; Joannopoulos, J. D.; Soljacic, M. Observation of unidirectional backscattering-immune topological electromagnetic states. *Nature* **2009**, *461*, 772−775.
(29) Wang, M.; Zhang, R. Y.; Zhang, L.; Wang, D.; Guo, Q.; Zhang, Z. Q.; Chan, C. T. Topological One-Way Large-Area Waveguide States in Magnetic Photonic Crystals. *Phys. Rev. Lett.* **2021**, *126*, No. 067401.
(30) Chen, J.; Li, Z. Y. Prediction and Observation of Robust One-Way Bulk States in a Gyromagnetic Photonic Crystal. *Phys. Rev. Lett.* **2022**, *128*, No. 257401.
(31) Noh, J.; Benalcazar, W. A.; Huang, S.; Collins, M. J.; Chen, K. P.; Hughes, T. L.; Rechtsman, M. C. Topological protection of photonic mid-gap defect modes. *Nat. Photonics* **2018**, *12*, 408−415.
(32) Lin, Z.-K.; Wang, Q.; Liu, Y.; Xue, H.; Zhang, B.; Chong, Y.; Jiang, J.-H. Topological phenomena at defects in acoustic, photonic and solid-state lattices. *Nat. Rev. Phys.* **2023**, *5*, 483−495.
(33) Barik, S.; Karasahin, A.; Flower, C.; Cai, T.; Miyake, H.; DeGottardi, W.; Hafezi, M.; Waks, E. A topological quantum optics interface. *Science* **2018**, *359*, 666−668.
(34) He, X. T.; Liang, E. T.; Yuan, J. J.; Qiu, H. Y.; Chen, X. D.; Zhao, F. L.; Dong, J. W. A silicon-on-insulator slab for topological valley transport. *Nat. Commun.* **2019**, *10*, 872.
(35) Shalaev, M. I.; Walasik, W.; Tsukernik, A.; Xu, Y.; Litchinitser, N. M. Robust topologically protected transport in photonic crystals at telecommunication wavelengths. *Nat. Nanotechnol.* **2019**, *14*, 31−34.
(36) Gao, X.; Yang, L.; Lin, H.; Zhang, L.; Li, J.; Bo, F.; Wang, Z.; Lu, L. Dirac-vortex topological cavities. *Nat. Nanotechnol.* **2020**, *15*, 1012−1018.
(37) Ma, J.; Xi, X.; Li, Y.; Sun, X. Nanomechanical topological insulators with an auxiliary orbital degree of freedom. *Nat. Nanotechnol.* **2021**, *16*, 576−583.
(38) Liu, W.; Hwang, M.; Ji, Z.; Wang, Y.; Modi, G.; Agarwal, R. Z2 Photonic Topological Insulators in the Visible Wavelength Range for Robust Nanoscale Photonics. *Nano Lett.* **2020**, *20*, 1329−1335.
(39) Luo, X. W.; Zhou, X.; Xu, J. S.; Li, C. F.; Guo, G. C.; Zhang, C.; Zhou, Z. W. Synthetic-lattice enabled all-optical devices based on orbital angular momentum of light. *Nat. Commun.* **2017**, *8*, 16097.
(40) Yuan, L.; Lin, Q.; Xiao, M.; Fan, S. Synthetic dimension in photonics. *Optica* **2018**, *5*, 1396−1405.
(41) Dutt, A.; Lin, Q.; Yuan, L.; Minkov, M.; Xiao, M.; Fan, S. A single photonic cavity with two independent physical synthetic dimensions. *Science* **2020**, *367*, 59−64.
(42) Ehrhardt, M.; Weidemann, S.; Maczewsky, L. J.; Heinrich, M.; Szameit, A. A Perspective on Synthetic Dimensions in Photonics. *Laser Photonics Rev.* **2023**, *17*, No. 2200518.
(43) Song, W.; Wu, S.; Chen, C.; Chen, Y.; Huang, C.; Yuan, L.; Zhu, S.; Li, T. Observation of Weyl Interface States in Non-Hermitian Synthetic Photonic Systems. *Phys. Rev. Lett.* **2023**, *130*, No. 043803.
(44) Yu, D.; Li, G.; Wang, L.; Leykam, D.; Yuan, L.; Chen, X. Moiré Lattice in One-Dimensional Synthetic Frequency Dimension. *Phys. Rev. Lett.* **2023**, *130*, No. 143801.
(45) Nguyen, D. H. M.; Devescovi, C.; Nguyen, D. X.; Nguyen, H. S.; Bercioux, D. Fermi Arc Reconstruction in Synthetic Photonic Lattice. *Phys. Rev. Lett.* **2023**, *131*, No. 053602.
(46) Li, G.; Wang, L.; Ye, R.; Zheng, Y.; Wang, D.-W.; Liu, X.-J.; Dutt, A.; Yuan, L.; Chen, X. Direct extraction of topological Zak phase with the synthetic dimension. *Light: Sci. Appl.* **2023**, *12*, 81.
(47) Javid, U. A.; Lopez-Rios, R.; Ling, J.; Graf, A.; Staffa, J.; Lin, Q. Chip-scale simulations in a quantum-correlated synthetic space. *Nat. Photonics* **2023**, *17*, 883−890.
(48) Cardman, R.; Raithel, G. Driving Alkali Rydberg Transitions with a Phase-Modulated Optical Lattice. *Phys. Rev. Lett.* **2023**, *131*, No. 023201.
(49) Nakata, Y.; Ito, Y.; Nakamura, Y.; Shindou, R. Topological Boundary Modes from Translational Deformations. *Phys. Rev. Lett.* **2020**, *124*, No. 073901.
(50) Lu, C.; Sun, Y. Z.; Wang, C.; Zhang, H.; Zhao, W.; Hu, X.; Xiao, M.; Ding, W.; Liu, Y. C.; Chan, C. T. On-chip nanophotonic topological rainbow. *Nat. Commun.* **2022**, *13*, 2586.
(51) Chen, X.-D.; Shi, F.-L.; Liu, J.-W.; Shen, K.; He, X.-T.; Chan, C.; Chen, W.-J.; Dong, J.-W. Second Chern crystals with inherently nontrivial topology. *Natl. Sci. Rev.* **2023**, *10*, No. nwac289.
(52) Xiao, M.; Zhang, Z. Q.; Chan, C. T. Surface Impedance and Bulk Band Geometric Phases in One-Dimensional Systems. *Physical Review X* **2014**, *4*, No. 021017.
(53) Wang, Q.; Xiao, M.; Liu, H.; Zhu, S.; Chan, C. T. Measurement of the Zak phase of photonic bands through the interface states of a metasurface/photonic crystal. *Phys. Rev. B* **2016**, *93*, No. 041415.
(54) Lu, C.; Wang, C.; Xiao, M.; Zhang, Z. Q.; Chan, C. T. Topological Rainbow Concentrator Based on Synthetic Dimension. *Phys. Rev. Lett.* **2021**, *126*, No. 113902.
(55) Silva, S. V.; Fernandes, D. E.; Morgado, T. A.; Silveirinha, M. G. Topological pumping and Tamm states in photonic systems. *Phys. Rev. B* **2022**, *105*, No. 155133.

https://doi.org/10.1021/acs.nanolett.3c04363
Nano Lett. 2024, 24, 1635−1641